Mechanical Properties of Laminate Materials: From Surface Waves to Bloch Oscillations

Z. Liang,[1] M. Willatzen,[2] and J. Christensen[2,*]

[1]College of Electronic Science and Technology, Shenzhen University, Shenzhen 518060, People's Republic of China

[2]Department of Photonics Engineering, Technical University of Denmark, DK-2800 Kongens Lyngby, Denmark

(Received 18 June 2015; revised manuscript received 28 July 2015; published 20 October 2015)

We propose hitherto unexplored and fully analytical insights into laminate elastic materials in a true condensed-matter-physics spirit. Pure mechanical surface waves that decay as evanescent waves from the interface are discussed, and we demonstrate how these designer Scholte waves are controlled by the geometry as opposed to the material alone. The linear surface wave dispersion is modulated by the crystal filling fraction such that the degree of confinement can be engineered without relying on narrow-band resonances but on effective stiffness moduli. In the same context, we provide a theoretical recipe for designing Bloch oscillations in classical plate structures and show how mechanical Bloch oscillations can be generated in arrays of solid plates when the modal wavelength is gradually reduced. The design recipe describes how Bloch oscillations in classical structures of arbitrary dimensions can be generated, and we demonstrate this numerically for structures with millimeter and centimeter dimensions in the kilohertz to megahertz range. Analytical predictions agree entirely with full wave simulations showing how elastodynamics can mimic quantum-mechanical condensed-matter phenomena.

DOI: 10.1103/PhysRevApplied.4.044012

I. INTRODUCTION

The boost experienced by acoustic and elastic (phononic) metamaterial research during the past years has been driven by the ability to sculpture the flow of sound waves at will. Motivated by the desire to engineer artificial structures in the form of metamaterials and the quest to map quantum-mechanical phenomena onto classical waves such as sound leads to many possibilities in material designs for control of wave motion and the potential for engineering applications. Once the specific wave physics is understood, one may think of its trivial extension to other types of waves. A wave, however, is simply not just a wave. Mechanical waves, which are elastic vibrations, can have one longitudinal polarization (like for acoustic sound waves in a gas or fluid) and two orthogonal transverse polarizations (like usually for electromagnetic waves). The freedom of three polarization directions, however, makes elastodynamics a rich discipline when trying to map wave physics from acoustics and electromagnetics (EM) to mechanical systems and vice versa [1,2].

In the past, structured phononic devices have provided rich insight to visualize with sound waves the classical analogues of a wide variety of quantum phenomena in atomic and condensed-matter physics. Many recent optical key findings have also inspired researchers to seek for their acoustic counterpart. As we mention above, vibrations, sound, and light propagate and interact by their own principles, and for this reason, the mapping between various systems might not always be possible.

Bloch oscillations (BOs) refer to wave packets that oscillate rather than translating through a crystal. This effect takes place when an electron is accelerated or slowed down by an external dc electric field up to the point of reaching the Brillouin edge [3]. The external field creates a gradient of the lattice potential that is responsible for the BO caused by multiple scattering, which is transferable to other types of waves and equivalent systems such as semiconductor superlattices [4], atomic systems [5,6], and photonic crystals [7–9]. Introducing a linear gradient of the effective refractive index in a plasmonic crystal is the optical analogue of a weak linear gradient of a lattice potential responsible for BOs [10,11]. Recent findings demonstrate how ultrasonic superlattices with a gradient of the cavity thicknesses can induce acoustic BOs [12–14]. Along a similar line, experimental observations of Wannier-Stark ladders and BOs were reported for longitudinal polarized elastic waves in porous silicon structures [15,16]. In the same context, we need also to mention that BOs have been experimentally detected in SAW cavities and phononic semiconductor multilayers [17,18].

In the microwave and terahertz regime, EM waves do not penetrate deep into the metal and are largely reflected. In order to mimic an effective penetration in the form of a decaying EM field into the metal equivalent of a surface mode, the perfect electric conductor is structured or pierced by apertures smaller than the vacuum wavelength [19,20].

*jochri@fotonik.dtu.dk

Recently, several works have shown that an equivalent acoustic surface mode running along a structured surface can be engineered and tuned by solely controlling the aperture size and material [21–24]. Other exciting effects such as the realization of acoustic parity-time symmetry and topological properties show that a vast amount of condensed-matter effects may be mapped to acoustics pushing this classical entity as close as possible to the complex realm of quantum mechanics [25–27].

In this article, we show how some of these ideas can be mapped to elasticity. As outlined above, mechanical waves are, in general, more complex as compared to EM and acoustics radiation making the transfer a nontrivial task. In combination with analytical insights and numerical computation, we derive geometrically induced dispersion relations of surface states between a fluid and solid-crystal half-space. The crystal under study is a 1D laminate material containing two stacked solids. This basis will later serve for understanding weakly coupled plate modes of varying thickness, akin to the oscillatory motions of electrons under the influence of a static electric field—mechanical BO.

II. DESIGNER SCHOLTE WAVES

The variety of different surface waves is broad depending on the materials surrounding the interface. Whether a solid-solid, fluid-fluid, or solid-fluid case is considered, waves have to attenuate or decay away from that interface along which it is confined. The excitation can be realized in many ways ranging from thermoelastic excitation to momentum-matched coupling [28–33]. Mechanical surface waves exist with different specific properties and are labeled Rayleigh, Scholte, and Stonely waves, just to mention the classical ones [34]. Their characteristics, that is, decay length or propagation speed, depend on the materials involved and are, therefore, not easily altered. However, in structured or layered media, the story is different. Here, one is able to tune surface waves dictated by the geometrical features [23,24]. Scholte waves, as an example, exist at a fluid-solid interface from which they decay as evanescent waves. In fact, this structure behaves very similarly to surface plasmons at a metal-dielectric interface. In order to acquire theoretical insight, we build an analytical model and conduct direct comparisons with rigorous numerical data. Consider a laminate material as depicted in Fig. 1(a). This uniaxial anisotropic structure exhibits hexagonal symmetry and is commonly labeled as horizontal transverse isotropy (HTI) media. On a macroscopic scale, one can construct such a structure by stacking two elastic solids along the x axis. No need to mention that the length scales need to be a fraction of the mechanical wavelength of interest to elucidate a metamaterial treatment.

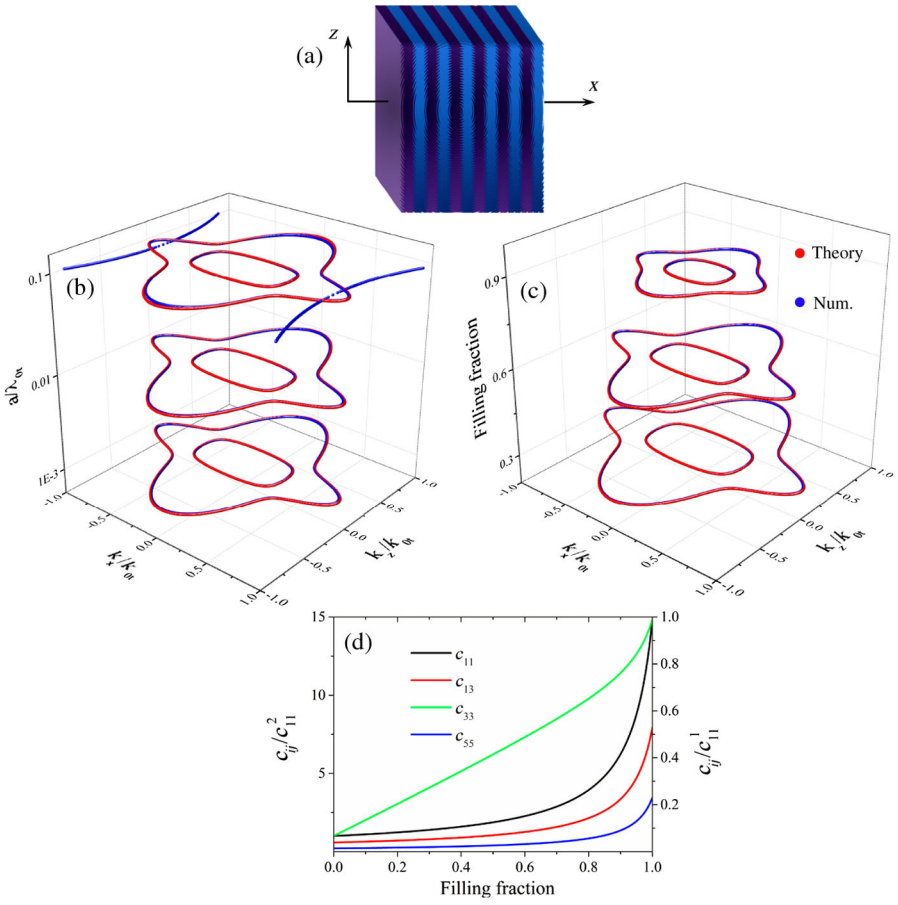

FIG. 1. Mechanical response of laminate materials. (a) Sketch of the basic structure composed of two stacked solids (aluminum and epoxy) of width h_1 and h_2 within the unit cell a. (b) The isofrequency contours are plotted for a filling fraction FF $= 0.5$. (c) Same as before, now, however, the frequency is fixed $a/\lambda_{0t} = 0.01$. (d) Effective stiffness as a function of filling fraction: right axis is normalized to the inclusion (medium 1) stiffness c_{11}^1, whereas the left axis is normalized to the background (medium 2) stiffness c_{11}^2.

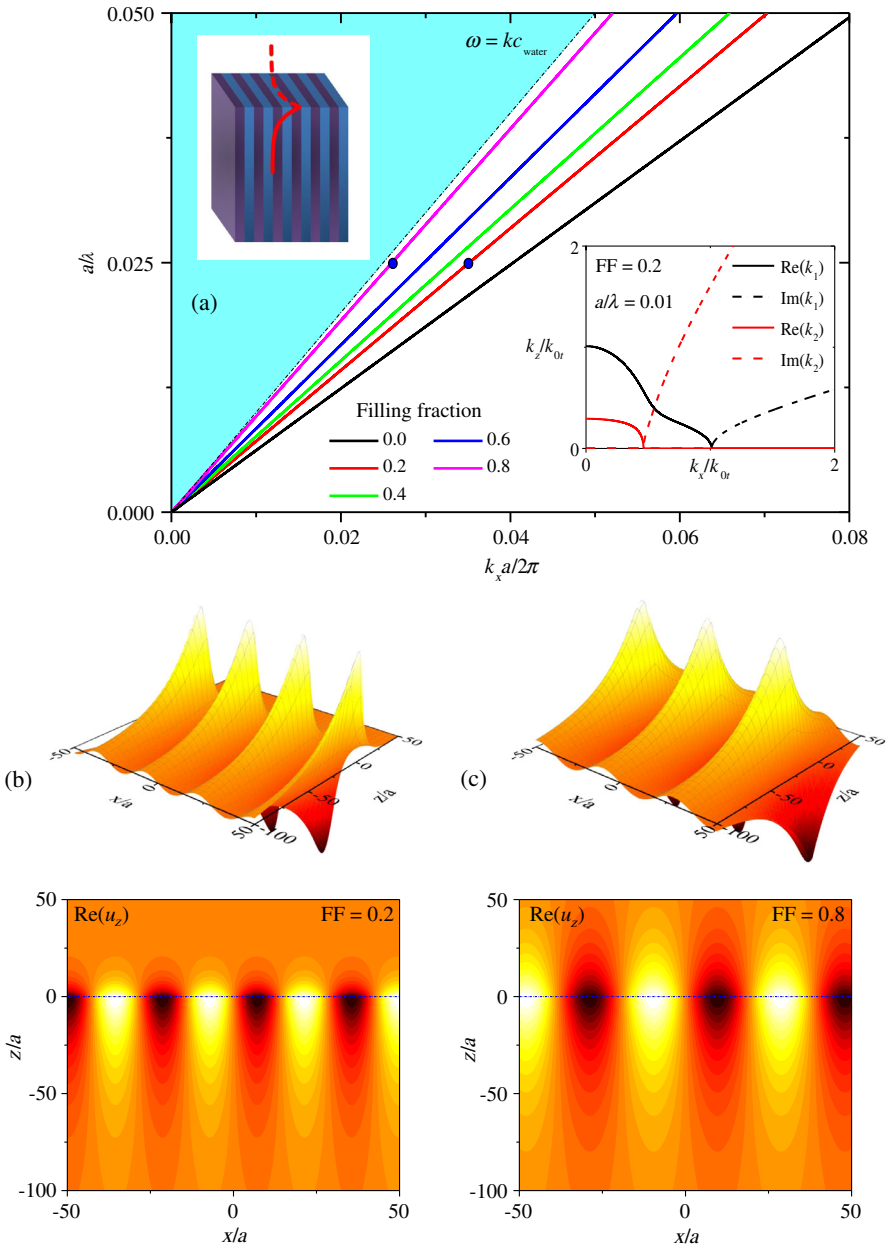

FIG. 2. Tunable designer Scholte waves. (a) A water-HTI medium interface is formed by various values of the crystal filling fraction, to which surface wave dispersion relations are plotted. The dotted line represents the sound line in water. Inset: Here we plot the isofrequency contours for both real and imaginary parts of the wave-number solutions. For (b) FF = 0.2 and (c) FF = 0.8 we map Re $= (u_z)$ at the water-HTI medium interface.

To represent the long-wavelength regime, we scale with the transversal wavelength $(\lambda_{0t} = 2\pi/k_{0t})$ of the background solid, medium 2. Any material can be chosen, and we take medium 1 (2) to be aluminum (epoxy) in the computed examples [35]. If mechanical vibrations are considered to take place only within the x-z plane (see Appendix A for details), a homogeneous linear system with the eigenpolarizations (U_x, U_z) can be expressed,

$$\begin{bmatrix} c_{11}k_x^2 + c_{55}k_z^2 - \rho\omega^2 & k_x k_z(c_{13} + c_{55}) \\ k_x k_z(c_{13} + c_{55}) & c_{55}k_x^2 + c_{33}k_z^2 - \rho\omega^2 \end{bmatrix} \begin{bmatrix} U_x \\ U_z \end{bmatrix} = 0, \tag{1}$$

from which all propagating modes can be computed. In passing, the solid mass density ρ and the four independent stiffness elements c_{ij} are effective ones, whereas k_x and k_z are the wave vectors along their respective axes. To answer the question whether we are able to derive analytical expressions for designer Scholte waves, we compute isofrequency contours as depicted in Fig. 1 for propagating modes where numerical and analytical treatments are compared. In Appendix A, the Christoffel equation is derived with effective parameters for a stacked HTI material as seen in Fig. 1(a). When writing out this equation, we arrive at Eq. (1), which when solved gives two solutions. The numerical method is based on plane-wave expansions along the periodicity direction and a harmonic wave along the perpendicular (z axis) direction leading to an eigenvalue system in k_z; see Appendix B. In what follows, we compare these two techniques by varying the normalized frequency

λ_{0t} and the filling fraction (FF) while determining the relation between k_x and k_z. We obtain two solutions, as can be seen in Figs. 1(b) and 1(c) that converge perfectly well with the numerical data for all selected cases. However, up to the limit where $\lambda_{0t} = 0.1$, that is, at the border of the long-wavelength regime, the numerical results predict more solutions that cannot be found with Eq. (1). Hence, for smaller frequencies, but for all possible filling fractions, our results confirm that the analytical treatment is exact. This finding lets us safely plot [see Fig. 1(d)] the effective stiffness moduli over the filling fraction where we normalize with c_{11} in each medium. Most important, this figure depicts how the mechanical properties can be tuned, but also, as expected, how $c_{11} = c_{33}$ when both isotropic limits (FF = 0 and FF = 1) are approached. Knowing the limitations, we can proceed with a fully analytical treatment into designer (spoof) mechanical surface waves of the Scholte type.

We have two solutions to Eq. (1) as we have seen before, and the same is true if all waves along z are evanescent; hence, as expressed with Eq. (C1), we seek surface wave solutions. With some material-specific definitions $\alpha_1 = c_{33}c_{55}$, $\alpha_2 = c_{33} + c_{55}$, and $\alpha_3 = c_{11}c_{33} - c_{13}^2 - 2c_{13}c_{55}$, the zero determinant of Eq. (C1) lets us solve for the wave numbers along the axis of wave decay:

$$k_z^2 = -\frac{\eta_1}{2\alpha_1} \pm \frac{\sqrt{\eta_1^2 - 4\alpha_1\eta_2\eta_3}}{2\alpha_1}. \tag{2}$$

In Eq. (2), we define $\eta_1 = \alpha_2\rho\omega^2 - k_x^2\alpha_3$, $\eta_2 = \rho\omega^2 - k_x^2 c_{11}$, and $\eta_3 = \rho\omega^2 - k_x^2 c_{55}$. Furthermore, we label the two solutions of k_z by $k_n = (k_1, k_2)$. Purely bound modes, as illustrated in the inset of Fig. 2(a), can be generated if the HTI structure is driven by an evanescent wave coming in from the fluid region that we choose to be water. As we elaborate in Appendix C, an effective response mimicking this behavior is achieved through the structured solid permitting acoustic and mechanical waves to decay in their respective regions. Consistent with the latter results, we take the HTI medium to be an aluminum-epoxy composite, although any solid can do the job. Imposing the right boundary conditions implies a dispersion relation for designer Scholte waves that entirely is controlled by the macroscopic composition

$$\frac{\omega^2\rho_0}{\beta} = -\frac{\Gamma_2 M_1 - \Gamma_1 M_2}{\tau_2 M_1 - \tau_1 M_2}, \tag{3}$$

where $\Gamma_n = k_x C_{13} - k_n\tau_n C_{33}$ and $M_n = k_n + k_x\tau_n$. Equation (3) gives rise to a linear dispersion of mechanical surface waves, which we demonstrate numerically in the following. Equation (3) is real and does not, therefore, add further numerical difficulties in the computation. Again, we modify the filling fraction, and as we see in Fig. 2(a), we obtain dispersion relations outside the sound cone that are evanescent but entirely linear. The slope of the bands and, hence, the degree of confinement, is tuned by the mixing of the two involved materials. Also, as plotted in Fig. 2(a), we see that k_n always gives rise to either fully real or imaginary solutions, meaning that we deal with purely bound modes and not attenuating ones. These designer surface waves with linear dispersion are broadband and can work for pulse signals. The degree of confinement that is controlled by the filling fraction is best illustrated by a field map. We lock the frequency at $\lambda = 40a$ and take two momenta $k_x = 2\pi 0.025/a$ and $k_x = 2\pi 0.035/a$ corresponding to FF = 0.8 and FF = 0.2, respectively. As shown in Figs. 2(b) and 2(c), we immediately observe that the decay length, as expected, is less pronounced the farther we lay outside of the sound cone. In this context we show how Scholte waves can be designed and entirely controlled by geometrical means. We note, however, as opposed to spoof surface plasmons, designer Scholte waves do not have a cutoff and are, therefore, weaker confined along the interface.

III. ELASTIC BLOCH OSCILLATIONS

The mechanical properties of laminate materials extend farther than classical surface waves, but such structures serve as a playground to demonstrate that elastic vibrations can map quantum-mechanical effects. Periodic oscillations of electrons in a solid subject to a constant driving field refers to a BO that has been recently observed for sound waves as well [12–14]. Hence, what is in fact possible to achieve with scalar fields (electrons and sound) is demonstrated in the following to be valid for vector problems such as elasticity problems. Again, we consider stacked laminates but containing plates of variable thickness h_i. The design of each plate is done assuming decoupled resonances. If the wave numbers k_i of the different plates (assigned index i) have a common denominator $k_{\min}$, then BOs for a coupled structure should result with wavelength

$$\lambda_{\mathrm{BO}} = 2\pi/k_{\min}. \tag{4}$$

Again, we consider mechanical vibrations to take place only within the x-z plane. To simulate uncoupled mechanical guides, we impose $T_{xz} = 0$ and $T_{zz} = 0$ at $z = \pm h_i$ corresponding to traction-free boundaries. These conditions allow symmetric (+) and antisymmetric (−) solutions

$$-\frac{\tan(q_t h_i)}{\tan(q_l h_i)} = \left[\frac{4k_i^2 q_l q_t}{(q_t^2 - k_i^2)^2}\right]^{\pm 1}, \tag{5}$$

where $q_l^2 = \frac{\omega^2\rho}{\lambda+2\mu} - k_i^2$ and $q_t^2 = \frac{\omega^2\rho}{\mu} - k_i^2$ correspond to longitudinal and transversal wave numbers, respectively. The determination of h_i requires solving Eq. (5) for fixed frequencies and predefined values in k_i, as we show below. We begin by assuming symmetric excitation only and determine the BO wavelength λ_{BO} by solving Eq. (5). This oscillation is composed of higher-ordered harmonics that are embedded into subsequent plates by gradually

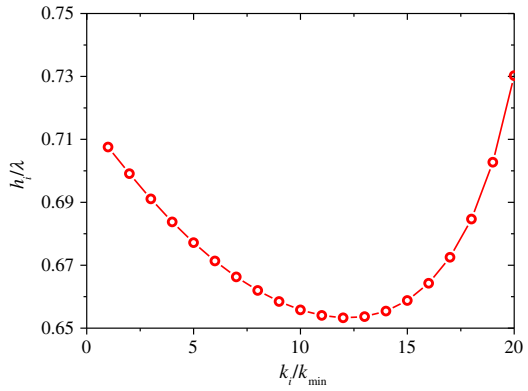

FIG. 3. Symmetric guided elastic plate modes for the case of copper with stress-free boundary conditions. The plate thickness h_i is normalized to the wavelength λ in water.

reducing the wavelength of individually guided elastic plate modes. Each subsequent symmetric wave number, therefore, increases along the stacking direction and can, thus, be evaluated by

$$k_i = N_i k_{\min}, \tag{6}$$

where N_i is an integer. In Fig. 3, we plot the evolution of $h_i(k_i)$. Note, a linear relationship is not essential; the most important ingredient is that k_i is a multiple integer of the fundamental BO mode. Such realization of a coupled plate system is an evenly spaced wave-number spectrum mimicking the Wannier-Stark ladder in wave-vector space. As an example, we take the plate material to be copper [35]. We stack the copper plates with an acoustic medium of large impedance contrast (water) so that only weak coupling between separate guides exists (tight-binding analogy). In principle, the distance between plates does not need to be constant but for efficient coupling, not too big. In the other extreme, all plates touching, BOs will be destroyed, but a wave will still propagate characterized by the thickness of all individual plates.

The symmetric excitation, for example, a Gaussian beam irradiation, will generate BOs according to the prescription given. In the idealized scenario, we employ vacuum conditions (traction-free boundary conditions) to treat the plates separately and uncoupled. To come close to that, as we mention above, we take water to be the background medium. As computed in Fig. 4 (COMSOL), if the plates are stacked relatively closely along the z direction to guarantee their interaction, a coupled wave spanning over the plates along the x direction is formed. This wave is characterized by the wavelength λ_{BO} as composed by the individual plates and their specific guided resonance k_i. To show this collective oscillation, we superimpose the function $\cos(k_{\min}x)$ that matches the full wave simulations exactly. Since sound waves are highly concentrated in the fluid region [see Fig. 4(a)], we plot $|u_x|$ within the solid region only so that the BO can be fully appreciated as illustrated in Fig. 4(b). Since we normalize all length scales by the

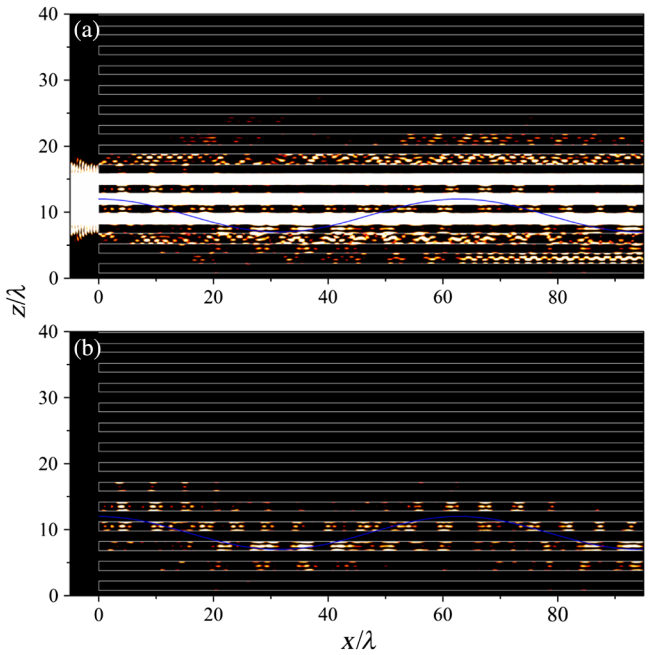

FIG. 4. Bloch oscillation in laminate materials. From the left side, we launch a fluid-borne acoustic Gaussian beam into the stacked copper plates that are surrounded by water. The displacement magnitude $|u_x|$ is plotted, (a) within the entire domain and (b) inside the elastic plates only. In both panels, we superimpose the fundamental BO $\cos(k_{\min}x)$. The length scale is normalized to the wavelength λ in water where $\lambda_{\mathrm{BO}}/\lambda = 20\pi$.

excitation wavelength, mechanical BOs could be experimentally observed at any scale, ranging from possible micrometer to centimeter measurements.

IV. CONCLUSIONS

In this work, we show a broad landscape of mechanical phenomena in laminate materials. With rather simple analytical techniques, we demonstrate how the concept of spoof surface plasmons can be mapped to elasticity. The same is true for BOs inspired by the well-known phenomenon in solid-state physics. We foresee that the tunability of designer Scholte waves can find interesting applications in mechanical wave guiding with the advantage of linear dispersion. Since the confinement of elastic vibrations at an interface can be designed at will, we expect many advantages in nondestructive techniques, sensing, and actuation. Certainly, one should be able also to sculpture surface vibrations in gap structures and particles made of these laminates. We provide a design recipe to describe how Bloch oscillations in classical structures of arbitrary dimensions can be generated, and we demonstrate this numerically for structures with millimeter and centimeter dimensions. Beyond the predicted generation of BOs, we expect to witness further mechanical analogies of electronic and plasmonic effects within a foreseeable time that should come to the attention of experimentalists.

ACKNOWLEDGMENTS

J. C. gratefully acknowledges financial support from the Danish Council for Independent Research and a Sapere Aude Grant No. 12-134776. Z. L. thanks for the support from Natural Science Foundation of SZU Grant No. 836-00008353 and No. 827-000030. We thank Jose Sanchez-Dehesa for stimulating discussions.

APPENDIX A: ANALYTICAL TREATMENT OF LAMINATE MATERIALS

The linear relationship between stress and strain is referred to as Hooke's law. In nonpiezoelectric materials when assuming small deformations, this relationship reads

$$T_{ij} = c_{ijkl} S_{kl} = c_{ijkl} \frac{\partial u_k}{\partial x_l}. \tag{A1}$$

c_{ijkl} is the rank-four stiffness tensor relating the second-rank tensors of the stress T_{ij} and strain S_{kl} between each other. The structure of interest is a HTI media; thus, Hooke's law can be written out as follows:

$$\begin{bmatrix} T_{xx} \\ T_{zz} \\ T_{xz} \end{bmatrix} = \begin{bmatrix} c_{11} & c_{13} & 0 \\ c_{13} & c_{33} & 0 \\ 0 & 0 & c_{55} \end{bmatrix} \begin{bmatrix} \varepsilon_{xx} \\ \varepsilon_{zz} \\ 2\varepsilon_{xz} \end{bmatrix}. \tag{A2}$$

c_{ijkl} is symmetric with respect to the suffixes l and k and lets us, in a simple way, express Hooke's law via the displacement u_k as shown in Eq. (A2). Upon neglecting gravity, the lossless and nonpiezoelectric equations of motion are

$$\rho \frac{\partial^2 u_i}{\partial^2 t} = c_{ijkl} \frac{\partial^2 u_k}{\partial x_j \partial x_l}. \tag{A3}$$

Alongside, in the elastostatics limit, the left-hand side of Eq. (A3) vanishes, and we are left with equations of equilibrium for a deformed body. Upon considering a monochromatic wave solution of polarization U_k,

$$u_k = U_k e^{i(k_0 n_j x_j - \omega t)} \tag{A4}$$

with $n_j = k_j/k_0$ denoting the unit slowness vector or wave-front normal where $k_0 = 2\pi/\lambda$ with the wavelength λ, we proceed by substituting Eq. (A4) into Eq. (A3). Using $U_i = \delta_{ik} U_k$, we arrive at the Christoffel equation

$$\left(\Gamma_{ik} - \delta_{ik} \frac{\rho\omega^2}{k_0^2} \right) U_k = 0, \tag{A5}$$

where $\Gamma_{ik} = c_{ijkl} n_j n_l$. Equation (A5) expresses a linear problem where $\rho\omega^2/k_0^2$ is the eigenvalue with corresponding eigenpolarizations U_k of the tensor Γ_{ik}. The solutions to the Christoffels equation, in general, give rise to three phase velocities with corresponding elastic polarization. In our 2D example, however, we have only two solutions.

The laminate material is constructed out of two isotropic material layers of widths h_1 and h_2 (the unit cell size is, therefore, $a = h_1 + h_2$ with filling fraction $\mathrm{FF} = h_1/a$. In layer 1 (2), we, therefore, denote the mass density ρ_1 (ρ_2) and the Lame coefficients λ_1 (λ_2) and μ_1 (μ_2), respectively. An effective medium theory can be expressed analytically by following the prescription by Postma [36]. The effective mass density is a classical length average,

$$\rho = \mathrm{FF}\rho_1 + (1 - \mathrm{FF})\rho_2, \tag{A6}$$

whereas the stiffness moduli follow some tight algebraic expressions,

$$\begin{aligned} c_{11} &= \frac{(h_1 + h_2)^2 (\lambda_1 + 2\mu_1)(\lambda_2 + 2\mu_2)}{D}, \\ c_{13} &= \frac{(h_1 + h_2)[\lambda_1 h_1 (\lambda_2 + 2\mu_2) + \lambda_2 h_2 (\lambda_1 + 2\mu_1)]}{D}, \\ c_{33} &= c_{11} + \frac{4 h_1 h_2 (\mu_1 - \mu_2)[(\lambda_1 + \mu_1) - (\lambda_2 + \mu_2)]}{D}, \\ c_{55} &= \frac{(h_1 + h_2)\mu_1 \mu_2}{h_1 \mu_2 + h_2 \mu_1}, \end{aligned} \tag{A7}$$

where

$$D = (h_1 + h_2)[h_1(\lambda_2 + 2\mu_2) + h_2(\lambda_1 + 2\mu_1)]. \tag{A8}$$

Note, if the stacking direction is vertical rather than horizontal, c_{11} and c_{33} have to be interchanged.

APPENDIX B: NUMERICAL TREATMENT OF LAMINATE MATERIALS

The numerical procedure to verify the solutions to the Christoffel equation comprising the effective stiffness moduli is based on a plane-wave expansion technique. We need to solve the general inhomogeneous form of the isotropic nonpiezoelectric wave equation:

$$\partial_j(\lambda \partial_i u_i) + \partial_i(\mu \partial_i u_j) + \partial_i(\mu \partial_j u_i) + \rho\omega^2 u_j = 0. \tag{B1}$$

By expanding out the material parameters and the eigensolutions on a basis of plane waves, which we will not detail any further here, one arrives at an eigenvalue system in k_z [37]:

$$\begin{bmatrix} C^{x,x}_{G,G'} - k_z^2 \mu_{G-G'} & -k_z C^{x,z}_{G,G'} \\ -k_z C^{z,x}_{G,G'} & C^{z,z}_{G,G'} - k_z^2 (\lambda_{G-G'} + 2\mu_{G-G'}) \end{bmatrix} \begin{bmatrix} u_x^{G'} \\ u_z^{G'} \end{bmatrix} = 0, \tag{B2}$$

where

$$C^{x,x}_{G,G'} = \rho_{G-G'}\omega^2 - (k_x + G)\times(k_x + G')(\lambda_{G-G'} + 2\mu_{G-G'}),$$
$$C^{x,z}_{G,G'} = (k_x + G)\lambda_{G-G'} + (k_x + G')\mu_{G-G'},$$
$$C^{z,x}_{G,G'} = (k_x + G')\lambda_{G-G'} + (k_x + G)\mu_{G-G'},$$
$$C^{z,z}_{G,G'} = \rho_{G-G'}\omega^2 - (k_x + G)\times(k_x + G')\mu_{G-G'}. \quad \text{(B3)}$$

After linearizing Eq. (B2), isofrequency contours can be computed.

APPENDIX C: DESIGNER SCHOLTE WAVES

We intend to model surface waves of the Scholte type between a fluid and a HTI structure. Similar to Eq. (1), we again write out the Christoffel equation, now, however, for modes decaying along the z axis:

$$\begin{bmatrix} c_{11}k_x^2 - c_{55}k_z^2 - \rho\omega^2 & -k_xk_z(c_{13} + c_{55}) \\ k_xk_z(c_{13} + c_{55}) & c_{55}k_x^2 - c_{33}k_z^2 - \rho\omega^2 \end{bmatrix}\begin{bmatrix} U_x \\ U_z \end{bmatrix} = 0. \quad \text{(C1)}$$

Defining the ratio of the polarizations in the system Eq. (C1), we reach

$$\frac{U_z}{U_x} = \tau_n = \frac{C_{11}k_x^2 - C_{55}k_n^2 - \rho\omega^2}{k_xk_n(C_{13} + C_{55})} = -\frac{k_xk_n(C_{13} + C_{55})}{C_{55}k_x^2 - C_{33}k_n^2 - \rho\omega^2}, \quad \text{(C2)}$$

where n stands for the number of solutions in $k_z = k_n = (k_1, k_2)$. We seek bound modes that are free to propagate along the entire interface [$z = 0$; see Fig. 1(a)] and decay away from it along z towards the fluid and the HTI region. In the elastic region, we write

$$u_x = (A_1e^{k_1z} + A_2e^{k_2z})e^{i(\omega t - k_xx)},$$
$$u_z = i(\tau_1A_1e^{k_1z} + \tau_2A_2e^{k_2z})e^{i(\omega t - k_xx)}, \quad \text{(C3)}$$

and in the fluid region we have

$$p = Be^{-\beta z}e^{i(\omega t - k_xx)},$$
$$u_z = -\frac{\beta}{\omega^2\rho_0}Be^{-\beta z}e^{i(\omega t - k_xx)}, \quad \text{(C4)}$$

where $\beta = \sqrt{k_x^2 - (\omega^2/c_0^2)}$ is the wave number along z. At the fluid-solid interface ($z = 0$), we apply the usual boundary conditions, namely, continuity of the normal displacements u_z in each region, continuity of the normal stress $p = -\sigma_{zz} = -C_{13}\partial_xu_x - C_{33}\partial_zu_z$, and zero shear stress $\sigma_{xz} = C_{55}(\partial_zu_x + \partial_xu_z) = 0$. These three conditions lead to equations of unknown wave amplitudes, which are written as follows:

$$\begin{bmatrix} k_xC_{13} - k_1\tau_1C_{33} & k_xC_{13} - k_2\tau_2C_{33} & i \\ \tau_1 & \tau_2 & -\frac{i\beta}{\omega^2\rho_0} \\ k_1 + k_x\tau_1 & k_2 + k_x\tau_2 & 0 \end{bmatrix}\begin{bmatrix} A_1 \\ A_2 \\ B \end{bmatrix} = 0. \quad \text{(C5)}$$

We find the solutions for this system by calculating the vanishing determinant, and after some straightforward algebra, we arrive at the dispersion Eq. (3) from the main text.

[1] G. W. Milton, *The Theory of Composites* (Cambridge University Press, Cambridge, England, 2002).
[2] J. Christensen, M. Kadic, O. Kraft, and M. Wegener, Vibrant times for mechanical metamaterials, MRS Commun. **5**, 453 (2015).
[3] F. Bloch, Uber die quantenmechanik der elektronen in kristallgittern, Z. Phys. **52**, 555 (1929).
[4] J. Feldmann, K. Leo, J. Shah, D. A. B. Miller, J. E. Cunningham, S. Schmitt-Rink, T. Meier, G. von Plessen, A. Schulze, and P. Thomas, Optical investigation of Bloch oscillations in a semiconductor superlattice, Phys. Rev. B **46**, 7252 (1992).
[5] M. B. Dahan, E. Peik, J. Reichel, Y. Castin, and C. Salomon, Bloch Oscillations of Atoms in an Optical Potential, Phys. Rev. Lett. **76**, 4508 (1996).
[6] M. Genske, W. Alt, A. Steffen, A. H. Werner, R. F. Werner, D. Meschede, and A. Alberti, Electric Quantum Walks with Individual Atoms, Phys. Rev. Lett. **110**, 190601 (2013).
[7] T. Pertsch, P. Dannberg, W. Elflein, A. Brauer, and F. Lederer, Optical Bloch Oscillations in Temperature Tuned Waveguide Arrays, Phys. Rev. Lett. **83**, 4752 (1999).
[8] R. Morandotti, U. Peschel, J. S. Aitchison, H. S. Eisenberg, and Y. Silberberg, Dynamics of Discrete Solitons in Optical Waveguide Arrays, Phys. Rev. Lett. **83**, 2726 (1999).
[9] R. Sapienza, P. Costantino, D. Wiersma, M. Ghulinyan, C. J. Oton, and L. Pavesi, Optical Analogue of Electronic Bloch Oscillations, Phys. Rev. Lett. **91**, 263902 (2003).
[10] W. Lin, X. Zhou, G. P. Wang, and C. T. Chang, Spatial Bloch oscillations of plasmons in nanoscale metal waveguide arrays, Appl. Phys. Lett. **91**, 243113 (2007).
[11] A. Block, C. Etrich, T. Limboeck, F. Bleckmann, E. Soergel, C. Rockstuhl, and S. Linden, Bloch oscillations in plasmonic waveguide arrays, Nat. Commun. **5**, 3843 (2014).
[12] H. Sanchis-Alepuz, Y. A. Kosevich, and J. Sanchez-Dehesa, Acoustic Analogue of Electronic Bloch Oscillations and Resonant Zener Tunneling in Ultrasonic Superlattices, Phys. Rev. Lett. **98**, 134301 (2007).
[13] Z. He, S. Peng, F. Cai, M. Ke, and Z. Liu, Acoustic Bloch oscillations in a two-dimensional phononic crystal, Phys. Rev. E **76**, 056605 (2007).
[14] A. A. Karabutov, Jr., Yu. A. Kosevich, and O. A. Sapozhnikov, Bloch oscillations of an acoustic field in a layered structure, Acoust. Phys. **59**, 137 (2013).
[15] Z. Lazcano, G. N. Aliev, and J. Arriaga, Experimental and theoretical demonstration of acoustic Bloch oscillations in porous silicon structures, J. Appl. Phys. **115**, 154505 (2014).

[16] Z. Lazcano and J. Arriaga, Acoustic Wannier-Stark ladders and Bloch oscillations in porous silicon structures, Appl. Phys. Lett. **105**, 231901 (2014).
[17] N. D. Lanzillotti Kimura, A. Fainstein, and B. Jusserand, Phonon Bloch oscillations in acoustic-cavity structures, Phys. Rev. B **71**, 041305(R) (2005).
[18] M. M. de Lima, Jr., Yu. A. Kosevich, P. V. Santos, and A. Cantarero, Surface Acoustic Bloch Oscillations, the Wannier-Stark Ladder, and Landau-Zener Tunneling in a Solid, Phys. Rev. Lett. **104**, 165502 (2010).
[19] J. B. Pendry, L. Martin-Moreno, and F. J. Garcia-Vidal, Mimicking surface plasmons with structured surfaces, Science **305**, 847 (2004).
[20] A. P. Hibbins, B. R. Evans, and J. R. Sambles, Experimental verification of designer surface plasmons, Science **308**, 670 (2005).
[21] S. Yao, X. Zhou, and G. Hu, Investigation of the negative-mass behaviors occurring below a cut-off frequency, New J. Phys. **12**, 103025 (2010).
[22] R. Hao, C. Qiu, Y. Ye, C. Li, H. Jia, M. Ke, and Z. Liu, Transmission enhancement of acoustic waves through a thin hard plate embedded with elastic inclusions, Appl. Phys. Lett. **101**, 021910 (2012).
[23] Z. Liang, M. Willatzen, J. Li, and J. Christensen, Tunable acoustic double negativity metamaterial, Sci. Rep. **2**, 859 (2012).
[24] J. Christensen, Z. Liang, and M. Willatzen, Metadevices for the confinement of sound and broadband double-negativity behavior, Phys. Rev. B **88**, 100301(R) (2013).
[25] R. Fleury, D. L. Sounas, and A. Alu, An invisible acoustic sensor based on parity-time symmetry, Nat. Commun. **6**, 5905 (2015).
[26] M. Xiao, G. Ma, Z. Yang, P. Sheng, Z. Q. Zhang, and C. T. Chan, Geometric phase and band inversion in periodic acoustic systems, Nat. Phys. **11**, 240 (2015).
[27] Z. Yang, F. Gao, X. Shi, X. Lin, Z. Gao, Y. Chong, and B. Zhang, Topological Acoustics, Phys. Rev. Lett. **114**, 114301 (2015).
[28] S. G. Joshi and R. M. White, Dispersion of surface elastic waves produced by a conducting grating on a piezoelectric crystal, J. Appl. Phys. **39**, 5819 (1968).
[29] M. F. Lewis, C. L. West, J. M. Deacon, and R. F. Humphreys, Recent developments in SAW devices, IEE Proceedings A, Physical Science, Measurement and Instrumentation, Management and Education, Reviews, **131**, 186 (1984).
[30] C. Desmet, V. Gusev, W. Lauriks, C. Glorieux, and J. Thone, Laser-induced thermoelastic excitation of Scholte waves, Appl. Phys. Lett. **68**, 2939 (1996).
[31] Y. Ye, M. Ke, Y. Li, T. Wang, and Z. Liu, Focusing of spoof surface-acoustic-waves by a gradient-index structure, J. Appl. Phys. **114**, 154504 (2013).
[32] J. Lu, C. Qiu, M. Ke, and Z. Liu, Directional excitation of the designer surface acoustic waves, Appl. Phys. Lett. **106**, 201901 (2015).
[33] D. J. Colquitt, R. V. Craster, T. Antonakakis, and S. Guenneau, Rayleigh-Bloch waves along elastic diffraction gratings, Proc. R. Soc. A **471**, 20140465 (2015).
[34] P. Hess, Surface acoustic waves, Phys. Today **55**, No. 3, 42 (2002).
[35] We use the following material parameters: $\mu = 2.63 \times 10^{10}\ \mathrm{N/m^2}$, $\rho = 2700.0\ \mathrm{kg/m^3}$, and $\lambda = 6.04 \times 10^{10}\ \mathrm{N/m^2}$ for aluminum, $\mu = 1.59 \times 10^{9}\ \mathrm{N/m^2}$, $\rho = 1180.0\ \mathrm{kg/m^3}$, and $\lambda = 4.43 \times 10^{9}\ \mathrm{N/m^2}$ for epoxy, $\mu = 4.10 \times 10^{10}\ \mathrm{N/m^2}$, $\rho = 8960.0\ \mathrm{kg/m^3}$, and $\lambda = 8.72 \times 10^{10}\ \mathrm{N/m^2}$ for copper, and $\rho = 1000.0\ \mathrm{kg/m^3}$ and $c_0 = 1500\ \mathrm{m/s}$ for water.
[36] G. W. Postma, Wave propagation in a stratified medium, Geophysics **20**, 780 (1955).
[37] M. S. Kushwaha, P. Halevi, G. Martinez, L. Dobrzynski, and B. Djafari-Rouhani, Theory of acoustic band structure of periodic elastic composites, Phys. Rev. B **49**, 2313 (1994).